Journal of Ceramic Processing Research. Vol. 23, No. 5, pp. 694~708 (2022)
(Received 9 April 2022, Received in revised form 23 June 2022, Accepted 25 June 2022)
https://doi.org/10.36410/jcpr.2022.23.5.694

J O U R N A L O F
Ceramic Processing Research

Review on preparation of zirconium carbide and boride ceramic powders

Faqi Zhan*, Hua Zhang, Ke Xv, Min Zhu, Yuehong Zheng and Peiqing La*
State Key Laboratory of Advanced Processing and Recycling of Nonferrous Metals, School of Materials Science & Engineering, Lanzhou University of Technology, Lanzhou 730050, China

This article summarizes and comments on the characteristics of zirconium carbide and boride powders synthesized by traditional synthesis methods. These methods include direct synthetic method, carbothermal reduction, magnesiothermic reduction, sol-gel, mechanical alloying, liquid phase precursor conversion, pre-ceramic polymers, and self-propagating high-temperature synthesis techniques. Additionally, this paper describes the latest research progresses of the self-propagating high-temperature synthesis (SHS) technique of zirconium carbide and boride, and prospects the nanocrystallization and large-scale will be the direction of future industrial researches.

Keywords: ZrC, ZrB_2, Nano powder, Synthesis methods, SHS technique.

Introduction

Many transition metal carbides and borides are ideal ultra-high temperature ceramics (UHTCs) [1, 2], such as HfB_2, ZrB_2, HfC, ZrC, and TaC, because of their high melting point (higher than 3000 °C), excellent physical and chemical properties, high electrical and thermal conductivity, good thermal shock resistance, moderate thermal expansion rate, high hardness and high strength under high-temperature conditions [3, 4]. Furthermore, they are not only applied in UHTCs but also have great potential in other fields [5]. Carbides are used in cutting tools, wear-resistant coatings, and the preparation of cemented carbide [6, 7, 8]. The excellent properties of borides make them a candidate material for a range of future applications such as hypersonic aircraft [9, 10], the molten metal crucible, furnace electrode, cutter, and wing leading edge [11]. However, a common problem of ultra-high melting point compounds is poor sintering property, which is mainly restricted by the purity and particle size of powders and has always been a hot and difficult point in the research of such materials [12]. Therefore, more and more attention has been paid to the preparation of ultrafine nano ceramic powders with excellent sintering properties.

It is worth noting that different preparation processes have a significant impact on some properties of zirconium carbide and boride powders (for example, particle size, purity, chemical reactivity, etc.), which will further affect the practical performances of the materials. This means that a better and advanced production process is needed, while the current preparation process is difficult to produce high-quality powder on a large-scale. At present, the following problems exist in the preparation of zirconium carbide and zirconium boride powders: poor purity, excessive oxygen content, uneven particle size, serious particle agglomeration, poor sintering performance, and small-scale, etc [13]. Therefore, how to prepare high-purity and nano ceramic powders on a large scale is an important challenge for us.

This article reviews on different preparation methods of zirconium carbide and zirconium boride, and summarizes the main factors on purity and particle size distribution, which lays a foundation for the synthesis of high-quality nano ceramic powders in the future.

Preparation Method of ZrC and ZrB_2

There are many preparation methods for carbides and borides. The conventional synthesis methods include direct elemental synthesis method [14], magnesium thermal reduction method [15], carbothermic reduction method [16], boron thermal reduction method [17], mechanical alloying method [18], self-propagating high-temperature synthesis method [19], sol-gel method [20], chemical vapor deposition method [21], spark plasma sintering [22], etc. Besides, liquid phase precursor conversion [23], pre-ceramic polymers [24], microwave synthesis [25], electric pulse synthesis and molten salt electrolysis [26], etc. can also be used.

Direct synthetic method

Using the corresponding elements in the target products as raw materials, the target products are directly obtained under high temperature in the inert gas atmosphere or

*Corresponding author:
Tel : +86-0931-2976688
Fax: +86-0931-2976688
E-mail: zhanfaqi@lut.edu.cn, pqla@lut.edu.cn

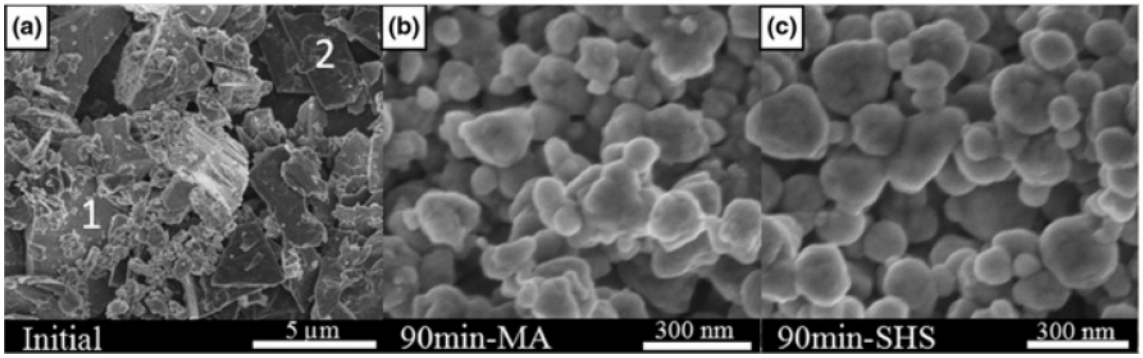

Fig. 1. Typical SEM images of: (a) initial Si/C powder mixture; (b) 90 min as-milled Si/C material at 17 G conditions (i.e., 650 rpm) and its corresponding combustion product (c) [28].

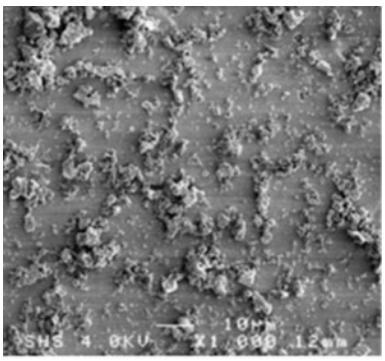

Fig. 2. SEM images of ZrB_2 and ZrC powders mixtures [29].

vacuum. The equation is as follows [27]:

$$Zr + C = ZrC \quad (1)$$

$$Zr + 2B = ZrB_2 \quad (2)$$

Mukasyan et al. [28] used this method to synthesize pure SiC nanopowders (size between 5 and 200 nm) in the Si + C system (Fig. 1). The biggest advantage of the direct synthesis method is that it is synthesized in one step, no by-products are generated, and the product purity is high. However, a higher reaction temperature and a certain raw material ratio are required, and the particle size of the product cannot be controlled.

Tsuchida et al. [29], under the condition of Zr:B:C = 2:2:1 (atomic ratio), mixed powders of ZrB_2 and ZrC were obtained by reaction in a graphite crucible (Fig. 2). The mixed powder is composed of sub-micron and <5 μm particles. The particles are fine and uniform with high purity, but the agglomeration of particles is serious.

This method has the advantage of high purity and simple synthesis condition. However, for powder products, the raw materials are expensive, the particle size is large, the agglomeration is serious, and the reactivity is low. For the process, the energy consumption is high, the cost is high, and industrial production is difficult. Therefore, it is only suitable for a small amount of high-purity preparations in the laboratory.

Carbothermal reduction method

The carbothermal reaction uses organic or inorganic carbon as a reducing agent to synthesize the target product through an oxidation-reduction reaction.

ZrC preparation reaction equation [30]:

$$ZrSiO_4 + 4C = ZrC + 3CO\uparrow + SiO\uparrow \quad (3)$$

$$ZrO_2 + 3C = ZrC + 2CO\uparrow \quad (4)$$

ZrB_2 preparation reaction equation [27]:

$$ZrO_2 + B_2O_3 + 5C = ZrB_2 + 5CO\uparrow \quad (5)$$

$$2ZrO_2 + B_4C + 3C = 2ZrB_2 + 4CO\uparrow \quad (6)$$

Zhou et al. [31] synthesized Zirconium carbide

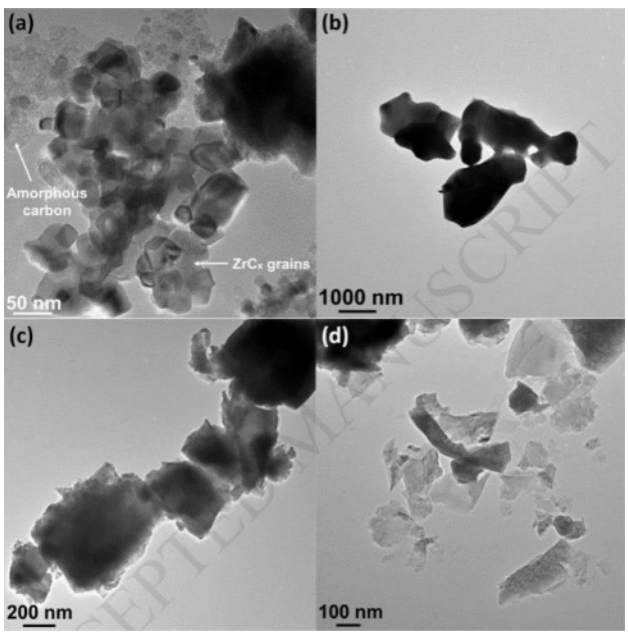

Fig. 3. TEM micrographs for ZrC_x powders synthesized using starting ZrH_2:C ratios of: (a) 1:0.98 after heating to 1300 °C, (b) 1:0.98 after heating to 2000 °C, (c) 1:0.60 after heating to 1300 °C, (d) 1:0.60 after heating to 2000 °C [31].

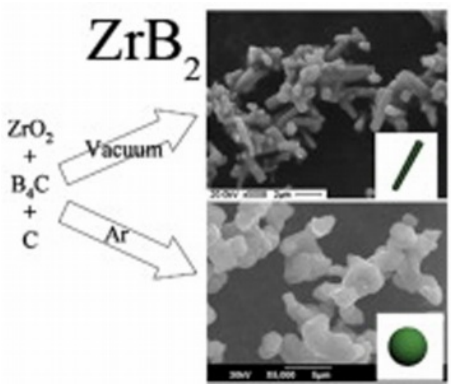

Fig. 4. ZrB_2 powders prepared by boro/carbothermal reduction of ZrO_2 under the different reaction atmosphere [32].

(ZrC_x) powder at 1300-2000 °C by reaction of zirconium hydride (ZrH_2) with carbon black in solid state. The crystal structure, lattice parameters and grain size of ZrC_x powders with ZrH_2: C starting ratio of 1:0.60 and 1:0.98 were characterized (Fig. 3). Crystallite sizes as small as about 50 nm were obtained due to the low synthesis temperature. Oxygen dissolved into the ZrC_x lattice when carbon vacancies were present.

Since the carbothermal reduction reaction is endothermic, it needs to provide heat from the outside to proceed, which will lead to the growth of crystal grains, and other technical means are usually required to control the particle size. Qiu et al. [32] prepared the ZrB_2 powders by boro/carbothermal reduction methods with different carbon source and reaction atmosphere. Results revealed that the carbon black as the carbon source led to a finer ZrB_2 powder compared with graphite in vacuum. In addition, vacuum atmosphere resulted in the formation of rod-like ZrB_2 powder, whereas argon atmosphere was conducive to form quasi-spherical ZrB_2 powder.

Chandran et al. [33] synthesized ZrB_2-SiC powders from different boron sources with coral-like micro-structure and an average particle size of 6.6 μm. When B_2O_3 is used as a boron source, the prepared ZrB_2 is porous and easily oxidized, but this problem can be effectively solved by using B_4C instead of B_2O_3 as a carbon source, so that it has a dense, oxidation-resistant glass film. However, the disadvantage of B_4C is that high adiabatic temperature will cause the particle size of ZrB_2 to become larger.

Lun et al. [34] synthesized nano ZrC powder by carbon thermal reduction of zirconia at 1600 °C. The prepared ZrC powder was fine and uniform, with a particle size of about 189 nm (Fig. 5) and oxygen content as low as 0.88 wt.%. The effects of low synthesis temperature, rapid heating and cooling rates, and electric current effectively inhibit particle growth.

The advantage of this method is that the equipment is simple and the process is mature. Low cost of raw materials and easy to control composition, such as zirconium carbon ratio. The disadvantages are high energy consumption, low yield, coarse product particles, and strict reaction control. Besides, when using boron oxide to produce ZrB_2, boron oxide is volatile and affects quality of products. When using boron carbide instead, the volatilization problem of boron oxide is solved, but the cost of boron carbide is high and the particle size is large.

Magnesium thermal reduction method

The magnesium thermal reduction method uses magnesium as a reducing agent to replace metal elements in metal oxides through reduction reactions, which are often used in industrial metallurgy. It is worth noting that a post-leaching treatment of the synthesis products is required to eliminate undesired phases.

ZrC was prepared by magnesium thermal reaction equation [35]:

$$ZrO_2 + C + 2Mg = ZrC + 2MgO \quad (7)$$

ZrB_2 was prepared by magnesium thermal reaction equation [36]:

$$ZrO_2 + \frac{1}{2}B_4C + \frac{3}{2}Mg = ZrB_2 + \frac{3}{2}MgO + \frac{1}{2}CO\uparrow \quad (8)$$

$$B_2O_3 + 5Mg + ZrO_2 = ZrB_2 + 5MgO \quad (9)$$

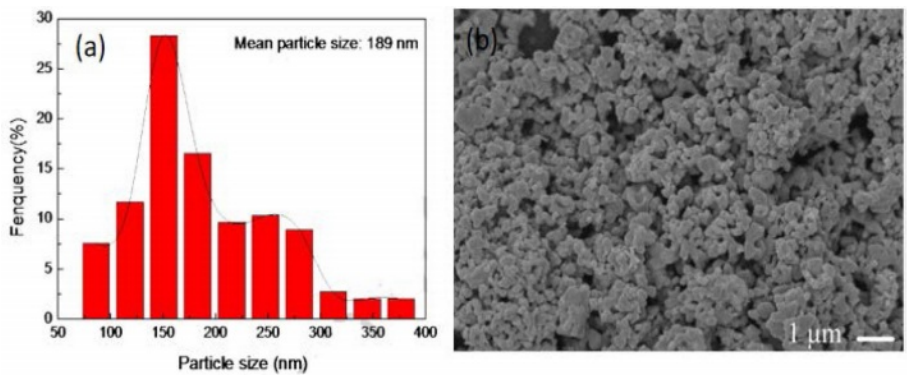

Fig. 5. (a) particle size distribution and (b) SEM image of ZrC powder synthesized by heating at 1600 °C for 2 h [34].

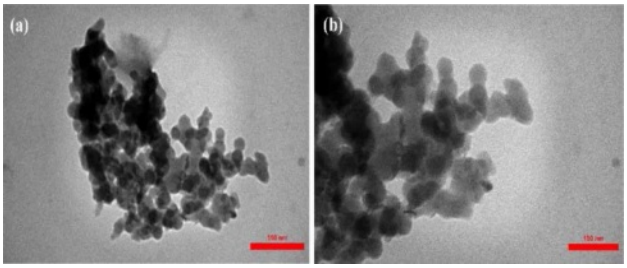

Fig. 6. TEM image of synthesized ZrB_2 [39].

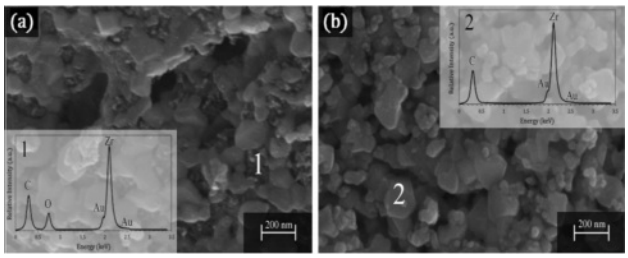

Fig. 7. SEM images and EDS spectra of ZrC sample heated in vacuum at: (a) 1200 and (b) 1400 °C [40].

The magnesium thermal reduction reaction will release a lot of heat. If the excess heat is not handled effectively, it will accelerate growth of grain and tend to agglomerate. The addition of endothermic substances can effectively absorb excess heat and achieve the purpose of grain refinement. La et al. [37] prepared ZrC powder with an average diameter of 46 nm, the specific surface area of 18.19 m^2/g, and high purity using zirconium oxide as zirconium source, carbon black as carbon source, and magnesium powder as reducing agent in NaCl-KCl mixed molten salts. The mechanism of NaCl-KCl is mainly phase-change endothermic and accelerated nucleation in liquid phase. Li et al. [38] used molten salt magnesium thermal reduction method to synthesize pure phase ZrB_2-SiC composite powder at 1200 ºC for 3 h. The results show that the reaction temperature and excessive Mg have an important influence on the synthesis of composite powder. The optimal values for determining n(B)/n(Zr) = 2.2, n(C)/n(Si) = 1.0, and excessive 50 wt.% Mg. The average crystallite sizes of ZrB_2 and SiC in the composite powder are about 500 and 30 nm, respectively. Emamalizadeh et al. [39] synthesized ZrB_2 nanopowders with different particle sizes and morphology by using low-temperature methane thermal reduction technology, magnesium metal powder as reducing agent and NaCl as diluent (Fig. 6). ZrB_2 particles are agglomerated, but the size distribution of nanoparticles is narrow, and the grain size is 11-69 nm.

Benefits of magnesium thermal reduction method: Replacement of expensive elemental metal with a metallic oxide can achieve cost reduction, mature processes, and convenient preparation process. The process of magnesium thermal reduction is exothermic, providing energy to the system, reducing extra energy consumption, the reaction process is fast and high efficient. Drawbacks: excessive heat can easily cause the grains to grow large and agglomerate, in addition to post-soaking treatment is required.

Sol-gel method

Sol-gel technology refers to the use of organic and inorganic metallic compounds as precursors. These precursors are evenly mixed in the liquid phase, followed by hydrolysis, condensation reactions, and ultimately heat treatment to form oxides or other compounds.

This method synthesizes the product through the pyrolysis of the organic precursor and widely used in the preparation of ultrafine powder. In the sol environment of the liquid phase, the product particles are uniform and regular. Arianpour et al. [40] chose zirconium acetate and sucrose as precursors of zirconium and carbon to synthesize irregular particles with a carbide phase less than 100 nm at 1400 °C in a vacuum, by combining sol-gel and carbothermic reduction (Fig. 7). Importantly, the optimal molar ratio of carbon to zirconium is 4:1, which gives the highest carbide content (96.6 vol.%) and lattice parameter (4.7003 Å).

Sol-gel method can not only control the particle size of the powder, but also has an important influence on the morphology of the powder. Zhang et al. [41] prepared ZrB_2 particles that were spherical by sol-gel method with different contents of water, and the average particle size decreased from 65 nm to 20 nm. In addition, with the increase of gelation temperature, the shape of particles changed from spherical particles at 65 ºC to chain particles at 75 ºC, and then formed rod particles at 85 ºC.

Significantly, it should be avoided to maintain a long time in the high reaction temperature range to prevent excessive growth of crystal grains. Miao et al. [42] using the Zr-B-C-O precursor(molar ratio of Zr:B:C is 1:4:20) is synthesized from the organic precursor of

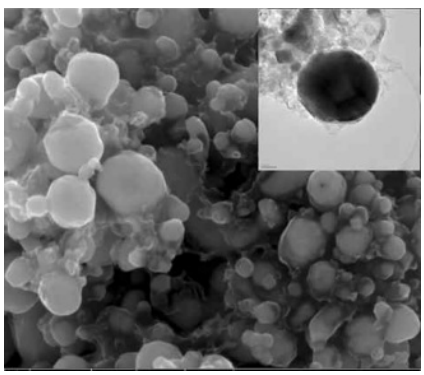

Fig. 8. SEM and TEM images of pyrolysis products in SPS heat treatment at 1700 °C for 5 min with Zr:B:C = 1:4:20 [42].

zirconium by the sol-gel method. Then, with the rapid synthesis of plasma sintering at 1700 °C for 5 min, successfully synthesized the pure phase ZrB_2 (Fig. 8).

The advantage of the sol-gel method is that the product quality is better, such as small particle size, low oxygen content, high chemical uniformity, large specific surface area, high reactivity, which is beneficial to sintering and subsequent processing. Usually, this method is used to prepare ultra-fine powder materials. However, it has shortcomings such as low production efficiency, many influencing factors, and complex operational processes.

Mechanical alloying (MA)

The process of solid-state alloying is realized by high energy grinding machine or ball mill. It is a complex physical and chemical process, the reaction mechanism is generally divided into two categories: one is the reaction mechanism about the gradual diffusion of atoms on the interface, and the second is the mechanism that the self-propagating reaction caused by the mechanical collision of the high-energy ball mill [18]. In the high-energy ball milling alloying reaction, the reaction product is usually an unbalanced product, which depends on the diffusion process, not on the overall composition. The second reaction mechanism is that when the particles reach the critical fine structure, the energy generated by the collision can induce the chemical reaction of the powder and release a lot of heat at the same time. This part of energy provides the power for further reaction. When the reaction is fully completed, the products generated should be in a stable equilibrium state. However, in the process of high-energy ball mill, strains, defects and nanoscale microstructure will be introduced, pushing the material away from the equilibrium state [27, 43].

The high-energy ball milling process can effectively improve the reactivity of the reactants and accelerate the reaction. It can crush large-sized particles, but it

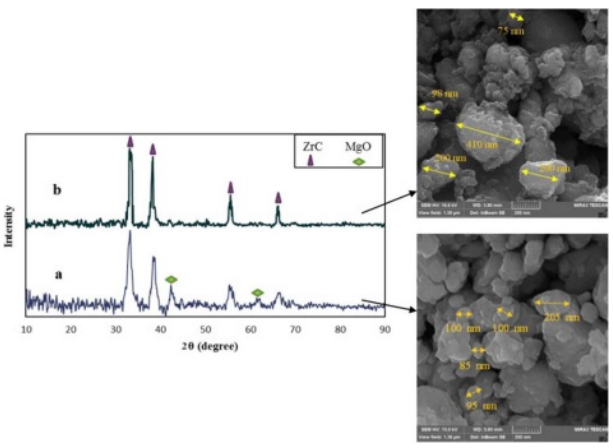

Fig. 9. X-ray diffraction patterns and FE-SEM images of the ZrC prepared by mechanochemical synthesis (30 h milled): (a) before leaching, (b) after leaching [44].

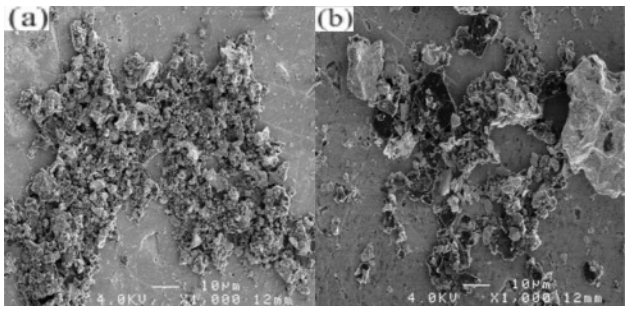

Fig. 10. SEM images of Zr:B:C = 1:1:1 samples obtained by (a) MA-SHS in air and (b) 1200 °C in argon [46].

can also cause uneven particle size distribution. Davoodi et al. [44] use the mechanochemical process in a high-energy ball mill to obtain nanostructured ZrC powder (Fig. 9). It can be seen that the size of the large particles is 410 nm, and that of the small particles is 75 nm, and the morphology is irregular.

If the reactivity of the product is too high, agglomeration will inevitably occur. Tabrizi et al. [45] used a mechanochemical combustion method to synthesize vanadium boride nano-powder in a high-energy ball mill. The grinding time was 100 min, and vanadium boride could be generated without further heating. The results show that the obtained vanadium boride agglomerates are composed of nano-scale initial particles with an average diameter of 36 nm. Takeshi et al. [46] used the powder mixture with Zr:B:C = 1:1:1 molar ratio to grind by planetary mill, spontaneous combustion, and high-temperature synthesis of ZrC and ZrB_2 occurred at the same time (Fig. 10). The results show that the high reactivity of disordered carbon formed by mechanical activation of graphite plays a decisive role. The product has obtained fine and uniform microstructure through MA-SHS in atmospheric environment, and is expected to become the precursor of ZrC-ZrB_2 composite.

The method can be used to prepare ultra-high melting point materials, the process is simple and efficient, and the product has high activity. However, because of the reaction caused by this mechanical impact, the particle size is uneven, easy to agglomerate, and impurities are introduced during the preparation process.

Liquid phase precursor conversion

Liquid phase precursor conversion method is to impregnate fiber preforms with precursor solution or molten solution, dry or solidify them under certain conditions, then pyrolysis at high temperature, and repeat the impregnation pyrolysis process for several times to obtain fiber-reinforced composites.

The agglomeration problem of the product prepared by this method is well alleviated. Wang et al. [47] synthesized nano ZrC powder by environmentally friendly aqueous solution method, using zirconium acetate and sucrose as raw materials, combined with

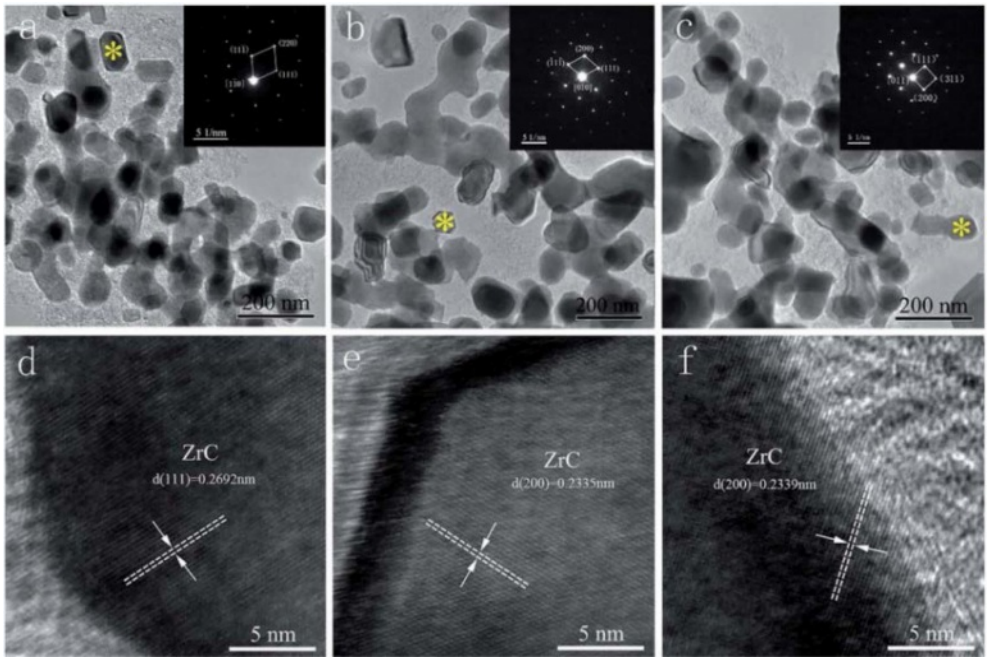

Fig. 11. TEM, HRTEM and SAED images of ZrC powder synthesized from precursors in different proportions [47].

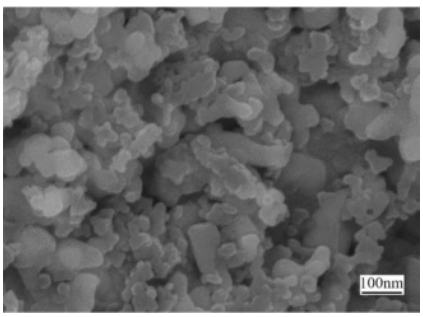

Fig. 12. SEM images of ZrB_2/ZrC/SiC ceramics [48].

polyvinylpyrrolidone (PVP), forming a highly stable ZrC precursor. The precursor can be converted into cubic ZrC by carbothermal reduction reaction at 1600-1650 °C. The SAED image reveals that the equiaxed particles are cubic ZrC (Fig. 11). The three powders show similar morphology and similar particle size, with an average particle size of 60 nm. The powder particles are dispersed and the degree of agglomeration is low.

Li et al. [48] prepared ZrB_2/ZrC/SiC liquid precursor using polyzirconia, boric acid and polymethyl silicon acetylene as raw materials by one-pot method. Nano-crystalline ZrB_2/ZrC/SiC ceramics were synthesized by pyrolysis in argon at 1400 °C. The results show that the ceramics are mainly composed of ZrB_2, ZrC and β-SiC phases with an average size of about 100 nm (Fig. 12). The oxidation of ZrC and ZrB_2 was inhibited by the presence of SiC at 1000 °C.

The preparation of carbide and boride powder by this method has simple equipment requirements and can greatly shorten the process period. It is a kind of preparation technology with great development potential. However, the organic solvents used in this method are harmful to human body and pollute the environment.

Pre-ceramic polymers (PCPs)

The method of hot cracking organometallic polymers into ceramics is suitable for the manufacture of ceramic materials with complex shapes such as films and fibers. Because of the meltable soluble organic metal polymer, the polymer chemical molding method, forming the polymer after the melting treatment (make the polymer crosslinking curing, change into a state of melting insoluble) and high temperature hot cracking, can be transformed into the corresponding shape of ceramic materials.

Due to the uniform atomic distribution of component elements, premixed polymer method is an effective method to synthesize ceramics at low temperature. Tao et al. [49] synthesized a new polymer-polyzirconoxanesal (PZS) from the reaction of zirconium oxychloride

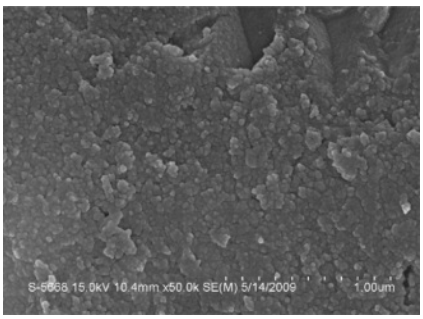

Fig. 13. SEM image of the synthesized ZrC powders at 1300 °C for 2 h [49].

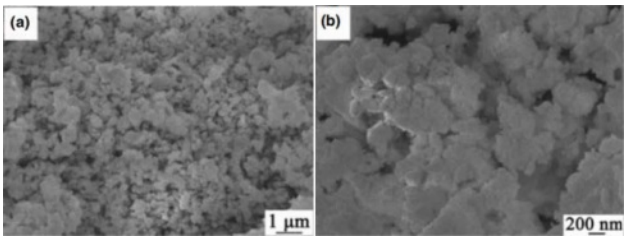

Fig. 14. SEM photos of ZrB_2 transformed from the precursor: (a) low magnification, (b) large magnification [50].

octahydrate ($ZrOCl_2 \cdot 8H_2O$) with acetylacetone (Hacac) and salicyl alcohol (SA) by one-pot protocol. Pyrolysis of this polymer at 1300 ℃ in argon provides nanosized ZrC with spherical morphology and size of 20-100 nm (Fig. 13).

Xie et al. [50] prepared ZrB_2 polymer precursors using $[(C_4H_8O)Zr(acac)_2]_n$ and $(NHCH_3)_3B_3N_3H_3$. During heat treatment in argon at 1500 ℃ for 2 h, the precursor with B/Zr molar ratio of 2 can be completely transformed into ZrB_2. The formed ZrB_2 particles are evenly distributed with a size of about 50-100 nm (Fig. 14). In addition, the formation of ZrB_2 particles is carried out through the liquid-phase reaction mechanism, and aggregation will occur in the pyrolysis process.

The process is used for the preparation of carbides and borides, one of the most important reasons is the potential reduction in manufacturing costs and relatively simple equipment requirements. However, agglomeration of the products will occur in different degrees during the pyrolysis process.

Self-propagating high-temperature synthesis (SHS)

The self-propagating high-temperature synthesis method, also known as the combustion synthesis technology, is a method for producing compounds by exothermic combustion reactions [51]. Reactions can occur between a solid reactant coupled with either gas, liquid, or other solid. This heat can supply the activation energy necessary for the reaction, which continues under the support of its exotherm until the combustion wave extends over the entire material. The reaction or combustion wave caused by combustion is quite fast, generally as 0.1-25.0 cm/s. The combustion reaction temperature is usually higher than 2100-3500 K. SHS relies on the energy self-sufficiency way to achieve the reaction between the initial ingredient. After ignition starts, external energy is no longer needed. Moreover, it can use cheaper raw materials to produce many products with high value-added and has good economic advantages. This method is an ideal method of large-scale preparation of refractory materials (including powders, metal alloys, ceramics, etc.), and the larger scale can achieve a better energy-saving effect. It should be noted that the combustion process has a large thermal gradient and cooling rate, which may lead to the formation of complex phases. Therefore, it is necessary to choose a reaction system that can meet the kinetic and thermodynamic requirements of the reaction.

The solid metal M and the solid non-metal X react to form a solid product MX, the calculation formula of its adiabatic temperature (T_{ad}) [52]:

$$\Delta H^0_{T_0} = \int_{T_0}^{T_{ad}} C_P(MX)dT$$

ΔH is the enthalpy of formation of MX at T_0 ($J \cdot mol^{-1}$), and Cp is the molar heat capacity of solid products ($J \cdot mol^{-1} \cdot K^{-1}$).

Since SHS depends on the heat provided by the system itself to maintain the reaction, the adiabatic temperature of the reaction system must meet its thermodynamic requirements. According to experience, self-propagating can be maintained spontaneously only at $T_{ad} \geq 1800$ K. In the calculation of the adiabatic temperature in the real reaction, the researchers will take into account the temperature change caused by the phase transition when the reaction temperature exceeds the phase transition temperature of the reagents.

Table 1. Advantages and disadvantages of the preparation methods

Methods	Advantages	Disadvantages
Direct synthesis	High purity, simple condition	Low reactivity, large particle size, serious agglomeration, high energy consumption, high cost
Carbothermal reduction	The equipment is simple, the technology is mature, the cost is low	High energy consumption, low yield, coarse particles, serious agglomeration
Magnesium reduction	Low cost, mature process, simple operation	Coarse particles, serious agglomeration, a post-leaching treatment
Sol-gel	The particle size is small, uniform, high purity, and high reactivity	Low efficiency, strict conditions, complex operation
MA	High reactivity, simple operation, simple equipment	Long cycle, low purity, non-uniform particles
Liquid phase precursor conversion	Low synthesis temperature, simple equipment and short cycle	Organic solvents are harmful and pollute the environment
Pre-ceramic polymers	Low manufacturing cost and simple equipment demand	Particle agglomeration
SHS	High purity, high reactivity, low cost, high efficiency	Particle agglomeration and process control difficulties

Table 2. Synthesis of ZrC-based ceramics.

Ref. #	Precursor	Process condition	Product quality
		Sol-gel technology	
1 [53]	$ZrOCl_2 \cdot 8H_2O$ + H_3BO_3 + Ethyl orthosilicate (TEOS) + glucose	Pyrolyzed at 1600 °C for 2 h	d_{ave}: ~220 nm, D50: ~255 nm, and d_{max}: ~5 μm.
2 [54]	$ZrOCl_2 \cdot 8H_2O$ + TEOS + Ethanol + Phenolic resin	C: (Zr + Si) = 7: (1 + 1) molar ratio, at 1600 °C for 1 h in Ar atmosphere.	ZrC-SiC, D50: ~0.174 μm. Adding phenolic resin, D50: ~0.255 μm.
3 [55]	Zirconium-(IV)-1-1-propanol (Zr $(OPr^n)_4$) + n-propanol + Toluene + Sucrose	Heated to 1495 °C at 10 °C·min^{-1} in Ar, with 3-30 min hold time.	d_{min}: ~30 nm, d: 30 ~40 nm, core-shell structure, and 5 nm Zr (C, O) shell. 5C: Zr (30 min) sample: d_{ave}: ~75 nm, and minor amounts of ZrO_2.
4 [56]	ZrO $(NO_3)_2$ + $Y(NO_3)_3$ + HNO_3 + Carbon black + hexamethylenetetramine (HMTA) + Urea	C/Zr =3, at 1550 °C for 4 h in argon containing 5%CO.	ZrO_2-ZrC-C (ZrCO) Crush strength: 0.51 kg/spheres Density: 2.28 g/cm^3. d_{ZrO2}: ~33 nm and d_{ZrC}: ~81 nm.
5 [57]	$ZrOCl_2 \cdot 8H_2O$ + TEOS + Sucrose + Ethanol	At 1500 °C for 1 h under vacuum, 12 vol.% SiC.	ZrC morphology: nearly spherical. D_{50}: ~268 nm. d_{min}: ~180 nm
6 [58]	Zirconyl oxychloride octahydrate (ZOO) + Gum Karaya + NaOH	Synthesized for 1 h at 1550 °C. a. GK-ZOO 1: 0.5 ratio b. GK-ZOO 1: 2 ratio c. GK-ZOO 1: 4 ratio	a. Exist unreacted carbon, large flaky particles (5~10 μm), and finer (<l μm) rough particles. b. No oxide phases present, d_{min}: ~40 nm, morphology: cubic structure. c. Exist unreacted m-ZrO_2, d_{ave}: ~800 nm, and morphology: Spherical particles.
7 [59]	$Ti(OC_4H_9)_4$ + $Zr(OC_4H_9)_4$ + C_4H_9OH + benzene-1.4-diol+ Acetylacetone (AcAc)	At 1600 °C in a vacuum.	Exist monoclinic ZrO_2 phase. d_{ave}: ~133 nm ± 32 nm TiC d_{ave}: ~50 nm ZrC d_{ave}: ~26 nm ZrO_2 d_{ave}: ~63 nm. Agglomerate d: 1~5 μm.
8 [60]	$ZrOCl_2 \cdot 8H_2O$ + Sucrose	Sucrose: The C:Zr = 3 molar ratio. Emulsifier: 0.1 wt.% of ZrO_2-gel. Blowing agent: 1 wt.% of ZrO_2. Curing agent: 1.5 wt.% of ZrO_2. At 1500 °C for 1 h under flowing argon atmosphere.	d_{ave}: ~175 nm.
9 [61]	Zirconium n-propoxide (ZNP) + AcAc + $C_5H_6O_2$ + ethanol + co-polymer surfactant (P123)	By Sol-Gel and Spark Plasma Sintering Method. P123: EtOH: AcAc: ZNP = 0.05:40:1, and Zr:C = 1:10 molar ratio, at 1750 °C for 5 min.	d: 100~500 nm.
		Direct synthesis	
10 [62]	ZrH_2 + carbon black	ZrH_2: C=1:0.6 molar ratio, at 1300 °C or 2000 °C.	ZrC_x with partially ordered vacancies, and particles were agglomerated, d: 50 nm~1000 nm.
		Self-propagating high-temperature synthesis.	
11 [25]	ZrO_2 + $C_{12}H_{22}O_{11}$ + Mg	40% endothermic rate. At 800 °C for 10 min under an argon.	Irregular shaped d_{ave}: ~50 nm, free C: 0.96 wt. %, O: 3.23 wt.%.
12 [63]	Zr + C	SHS: at 2390 ± 80 °C, after 5-20 milling. SPS: at 1850 °C for 20 min, 50 MPa	d_{ave}: 12.5-5 μm, Vickers hardness: 17.5 ± 0.4 Gpa, Fracture toughness: 2.6 ± 0.2 MPa·m$^{0.5}$, Mechanical strength: 250 MPa.
		Carbothermal reduction	
13 [64]	ZrO_2 + phenolic resin	SPS + carbothermal reduction Molar ratio (C/Zr) = 3.6, 800 °C pyrolysis.	d_{ave}: ~200 nm, and O: 0.49 wt.%.
14 [34]	ZrO_2 + Phenolic resin	SPS + carbothermal reduction Molar ratios (C/Zr) = 3.6, at 1600 °C for 2 h.	d_{min}: ~189 nm, O: 0.88 wt.%, and Purity: 99.87%.
15 [65]	ZrO_2 + TiO_2 + graphite	At 1400 °C for 1 h. Ti/Zr = 6:4.	TiC-ZrC d_{ave}: ≤ 250 nm.
		Mechanochemical synthesis.	
16 [66]	ZrO_2 + NiO + Mg + C	Powder: ball = 1:20 at 600 rpm under argon. M2: pre-activated for 6 h. M3: extra 30 wt.% graphite.	ZrC-Ni composite powders M2: d_{ave}: 42 ± 4 nm, and spherical morphology. M3: d_{min}: 30 ± 3 nm, and morphology: entirely spherical.
17 [44]	ZrO_2 + graphite + Mg	ball: powder = 20:1, 600 rpm, time: 30 h	Morphologies: spherical and irregular. d_{ave}: ~45 nm. Agglomerated d_{ave}: ~300 nm.

Table 2. Continued.

Ref. #	Precursor	Process condition	Product quality
		Liquid phase synthesis	
18 [67]	PZC + LPCS	LPCS: PZC = 1: 1 mass ratio, at 1550 °C in argon.	ZrC-SiC: two phases are uniformly distributed, and spherical morphology. d_{ave}: ≤ 60 nm.
19 [47]	ZrO $(CH_3COO)_2$ + $C_{12}H_{22}O_{11}$ + polyvinyl pyrrolidone (PVP)	ZrO $(CH_3COO)_2$: $C_{12}H_{22}O_{11}$ = 4:1.5, at 1650 °C.	*d*: 50 ~100 nm, d_{ave}: ~56 nm, and O: ≤ 1.0 w%.
		Chemical vapor deposition (CVD)	
20 [68]	ZrO_2 + CH_4	Optimal CVD conditions: 1300 K, 30 minutes, C deposit (23 wt.%). At 1800 K, 120 minutes.	O: 0.59 wt.%, and d_{ave}: ~170 nm.
		Other advanced techniques	
21 [69]	$ZrSiO_4$ + carbon black	A one-pot electrolytic process $ZrSiO_4$/C (3 wt.% C), under 3.1 V at 850 °C for 20 h in eutectic $CaCl_2$-NaCl melt.	ZrC/ZrSi: multicore-shell structure. ZrC *d*: 10~40 nm.
22 [70]	ZrO_2 + carbon black	Microwave synthesis. Microwave field: 2.45 GHz, at 3 kW for 50 min, T_{max}: 1400 °C.	d_{ave}: ≤100 nm, and spherical morphology.

Note: *d* = Particle size range, d_{ave} = Average particle size, d_{min} = Minimum particle size, d_{max} = Maximum particle size, D50 = median diameter.

Besides, the volatilization loss of the reactants, the particle size of the raw materials, molding pressure, protective atmosphere, etc., all have an impact on the reaction. Therefore, controlling these variables is of great significance for the preparation of high-quality powders. However, the SHS reaction time is very short, which makes process-controlling been a hot and difficult point of self-propagating high-temperature synthesis technology.

Each preparation method has its advantages and disadvantages, which are summarized in the Table 1. The specific examples of ZrC and ZrB_2-based ceramics

Table 3. Synthesis of ZrB_2-based ceramics.

Ref. #	Precursor	Process condition	Product quality
		Boro/Carbothermal Reduction Method	
1 [71]	ZrO_2 + B_4C + C	ZrO_2:B_4C:C = 1:0.6:1.5, heated to 1650 °C, vacuum, and heating rate: 10 °C per minute.	*d*: 0.9~1.03 μm
2 [72]	$ZrOCl_2 \cdot 8H_2O$ + B_4C + C	Raw materials in 2: 1.2: 3 M ratio, temperature: 1600 °C held for 60 min.	Rod-like ZrB_2 *d*: 0.5~3 μm, and high aspect ratios of >8.
3 [73]	ZrO_2 + Sodium metaborate (HBO_2) + Carbon black	HBO_2: 60 wt.%, at 1600 °C in Ar atmosphere, and adding 30 wt.% NaCl.	Pure ZrB_2 powders, and hexagonal structure, *d*: 1~2 μm.
4 [2]	ZrO_2 + B_4C	Heat-treated: 1250 °C in flowing argon, B_4C: 1.1~1.4 M ratio.	O: 0.14% and C: 0.3%. *d*: 5 μm(1.4) to 245 nm(1.1).
5 [74]	$ZrSiO_4$ + B_2O_3 + Mg + C	a. Using expanded graphite at 1550 °C. b. Using carbon black at 1500 °C.	a. ZrB_2: regular hexagonal shape, d_{ave}: ~2.0 μm. SiC: whisker-shaped, d_{ave}: ~0.15 μm and aspect ratio: > 20. b. Morphologies: granular and short rod-shaped, and *d*: 0.2 μm~0.6 μm.
6 [75]	ZrO_2 + B + Mg	The first step: 20% excess amount of Mg. The second step; heat-treated, Mg:ZrB_2 = 10:1 mass ratio.	The first step: O: 2.40 wt.%, d_{ave}: ~0.53 μm and D50: ~0.3636 μm. The second step: O: 0.50 wt.%, d_{ave}: ~0.54 μm and D50: ~0.42 μm.
7 [76]	ZrO_2 + B_4C + C	ZrO_2:B_4C:C= 2:1:3 At 1600-1700 °C	d_{ave}: 10.9-12.9 μm, Specific surface area: 1.8-3.6 m^2g^{-1}
		A molten-salt-assisted mothed	
8 [77]	ZrO_2 + $Na_2B_4O_7$ + Si	At 1200 °C for 3 h, and the addition of 20 wt.% Si.	Morphology: sheet-like, d_{ave}: ~0.7 μm.
9 [78]	ZrO_2 + Amorphous B + NaCl	At 1223 K for 3 h, NaCl/Reactant = 0.25 mass ratio, and ZrO_2:B = 3:10 molar ratio.	d_{ave}: ~500 nm.
10 [79]	$ZrOCl_2 \cdot 8H_2O$ + $Na_2B_4O_2 \cdot 10H_2O$ + $C_{l2}H_{22}O_{11}$ + NaCl	Zr:B:C = 1:5:5 At 1400 °C for 4 h	d_{ave}: 1~2 μm, and aspect ratios of 3~10.

Table 3. Continued.

Ref. #	Precursor	Process condition	Product quality
		Synthesis by solid solution	
11 [80]	ZrO_2 + Ta_2O_5 + Amorphous boron + SiC	ZrO_2 + 2.6 mol.% Ta_2O_5 + B, at 1000 °C/2 h and then 1550 °C/1 h.	$Zr_{0.95}Ta_{0.05}B_2$ d_{ave}: < 0.5 μm
12 [81]	ZrO_2 + B + TiO_2	Addition of 10 mol% TiO_2, at 1550 °C for 1 hour.	d_{ave}: ~0.37 μm.
		A sol-gel method	
13 [82]	$ZrCl_4$ + H_3BO_3 + TEOS + Novolac resin	B:Zr = 2.5 and C:Zr = 3, at 1470 °C in argon for 1 h.	d_{ave}: < 250 nm, specific surface: 81.479 m^2 g^{-1}.
14 [83]	$[(C_4H_8O)\ Zr(acac)_2]_n$ + $[(NHCH_3)_3B_3N_3H_3]_n$ + Polycarbosilane	ZrB_2:SiC = 1:4.	Zr-containing spheres At 1700 °C *d*: 200~300 nm. At 1500 °C *d*: ~100 nm.
15 [84]	$ZrOCl_2 \cdot 8H_2O$ + H_3BO_3 + TEOS + $C_6H_{12}O_6 \cdot H_2O$ + $C_6H_8O_7 \cdot H_2O$ + $C_2H_6O_2$	Precursor: at 353 K for 5-7 h, gel: oven-dried at 373 K for 24 h, heated to 1273 K (20 K/min), and then 1573 K (10 K/min) for 3 h.	ZrB_2-SiC d_{ave}: ~35 nm. Agglomeration d_{ave}: ~9 μm.
16 [85]	ZrO_2 + H_3BO_3 + Carbon black + SiC	ZrO_2:H_3BO_3:C = 1:3.6:5, adding 30 vol.% SiC, at 1500 °C for 90 min.	Regular columnar ZrB_2 *d*: 1~2 μm.
		SHS method	
17 [86]	Al +Zr + W + B_2O_3	a. B_2O_3:Al:Zr:W:B =2:2:3.5:1:1 b. B_2O_3:Al:Zr:W:B =2:2:2.5:2:0 c. B_2O_3:Al:Zr:W:B =3:2:4:4:0	Composite phase structure: Al_2O_3-ZrO_2, Al_2O_3, and ZrO_2, WB, ZrB_2. a. d_{ave}: ~135 mm. b. d_{ave}: ~143 mm. c. d_{ave}: ~167 mm.
18 [87]	Zr + Ta + B	At 2000-2100 °C Adding extra boron	ZrB_2 d_{ave}: ~6.7 mm, BET: 1.09 m^2/g TaB_2 d_{ave}: ~1.5 mm, BET: 1.16 m^2/g
		Mechanical alloying	
19 [88]	ZrO_2 + B_2O_3 + C	At 1750 °C, and ZrO_2:B_2O_3:C = 1:4.5:7.5.	d_{ave}: ~67 nm.
		Other advanced techniques	
20 [89]	$ZrSiO_4$ + H_3BO_3 + C	A microwave synthesis. $ZrSiO_4$:H_3BO_3:C = 1:2.6:8, and at 1500 °C.	Short columnar-like ZrB_2, and SiC whiskers. d_{ave}: < 1 μm.
21 [90]	ZrO_2 + B_2O_3 + Na	ZrO_2:B_2O_3:Na = 1:1:5 at 873 K.	d_{ave}: 0.1 μm.
22 [91]	$ZrOCl_2 \cdot 8H_2O$ + $Na_2B_4O_7 \cdot 10H_2O$ + $C_{12}H_{22}O_{11}$ + Si	Situ synthesis At 1300 °C for 2 h and then at 1400 °C for 2 h.	Rod-shaped ZrB_2, aspect ratio: > 8, d_{ave}: ~300 nm.

Note: *d* = Particle size range, d_{ave} = Average particle size, d_{min} = Minimum particle size, d_{max} = Maximum particle size, D50 = median diameter.

prepared by different methods are summarized in Table 2 and 3.

Research Status of Self-propagating High-temperature Synthesis

Since the self-propagating high-temperature synthesis technology was proposed by Merzhanov et al. [92, 93] in 1967, it has been explored and researched for half a century [94]. So far, it has been used in many fields [95], such as self-propagating high-temperature synthesis of carbides, nitrides, borides, oxides, composite oxides, superconductors, alloys, and other materials [96].

Self-propagating high-temperature synthesis of zirconium carbides

To reduce the excessive heat generated in the self-propagating process, the researchers reduced the T_{ad} value by adding different content of diluents and studied the effects of different carbon sources (graphite, activated carbon, black carbon). Li et al. [97] prepared particle size of 0.5-1 μm ZrC powder by adding sodium chloride (5 wt.%-30 wt.%) as a diluent in the Zr-C system. The results show that when the carbon source is black carbon, a product with a lower oxygen content (0.38 wt.%) can be obtained. As the diluent content increases, the adiabatic temperature of the reaction system decreases. When NaCl is increased to 30 wt.%, the adiabatic temperature of the reaction system is reduced to 1810 K, and ZrC ultrafine powder of 50 nm can be obtained. Through the above research, the results show that the use of sodium chloride as a diluent will not reduce the purity of the product, and the obtained powder has a smaller particle size and a better morphology. It is worth noting that the total amount of powder prepared in this study is relatively small. In addition, there is a lack of research on the mechanism of the diluent NaCl.

To further improve the product quality, researchers control the reaction process by adjusting the endothermic rate of the reaction. Da et al. [25] used traditional cheap zirconium dioxide powder (ZrO_2), magnesium (Mg), and sucrose ($C_{12}H_{22}O_{11}$) as raw materials. The synthesized ZrC nanopowder has high purity, low oxygen content, uniform distribution, and an average particle size of 50 nm (Fig. 15). Besides, because sucrose decomposition and carbothermal reduction are endothermic, the adiabatic temperature can be reduced by controlling the proportion of endothermic reaction in the system. However, as a reducing agent, magnesium occupies a large proportion in the system, and its melting and volatilization also have a great influence on the thermal effect of the system [93]. Therefore, the study lacked research on the amount of magnesium added.

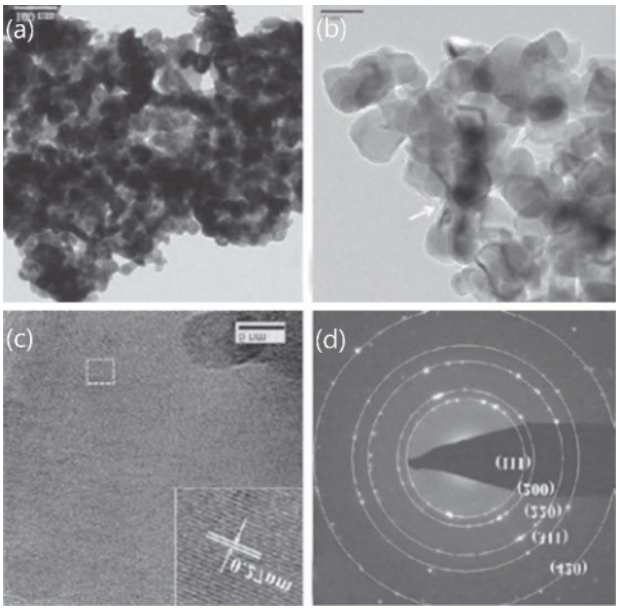

Fig. 15. Typical TEM (a, b), HRTEM (c), and SAED (d) images of ZrC powder was prepared when the heat absorption rate was 40%. [25].

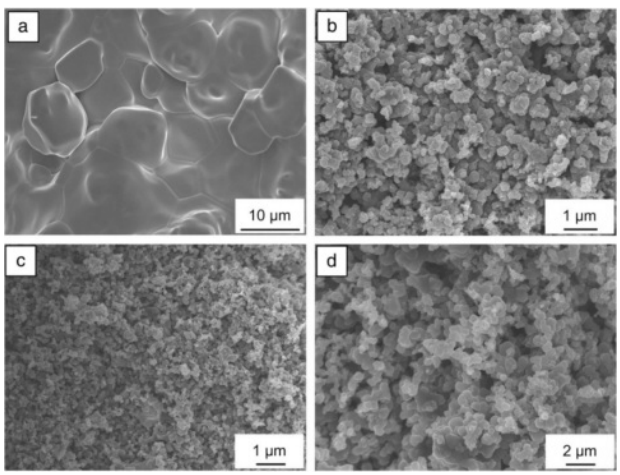

Fig. 16. Microstructures of SHS products with (a) 0, (b) 10, (c) 20 and (d) 30 wt.% Cu-Zr-C reactants, respectively [98].

In addition, the research of adding metal powders such as Cu, Al and Fe into reactants to promote and accelerate the reaction and synthesize carbides by pre forming liquid at low temperature has also attracted a lot of attention. Zhang et al. [98] successfully prepared ZrC particles by adding different contents of Cu to zirconium carbon powder mixture through combustion synthesis technology (Fig. 16). In Cu-Zr-C system, Cu additive plays an important role in reaction behavior and formation pathway. It not only inhibits the growth of ZrC particles, but also participates in and promotes SHS Reaction.

Self-propagating high-temperature synthesis of zirconium borides

The researchers studied the macro-kinetic characteristics of the combustion of the Ta-Zr-B system and the mechanism of chemical reactions and phase formation in the combustion wave. Kurbatkina [99] synthesized refractory boride ceramics (Zr, Ta)B_2 with excellent properties through SHS. It is found that the combustion has the characteristics of a spin mode, which indicates the restriction effect of gas-phase mass transfer on the reactants. The researchers detected tantalum and zirconium as the main solid solutions in the preheating zone, and the temperature in this zone was lower than the melting point of the reactants. After the zirconium and boron melt, the temperature in the combustion zone reaches the highest. Zirconium diboride (1-3 μm) is precipitated from the supersaturated solution (Fig. 17), which is then hot-pressed into a dense ultra-high temperature ceramic (UHTC). The highest hardness of boride ceramics is 70 GPa, Young's modulus is 594 GPa, and the elastic recovery rate is 96%. The thermal conductivity of (Zr, Ta)B_2 is 35-42 W/mk. The plasma torch test showed that the obtained ceramic has high oxidation resistance at 2900-3000 °C. It can be seen from Fig. 17 that the particles agglomerate seriously. The study found that the combustion temperature is 3451 K. Excessive temperature will cause particle agglomeration. Therefore, it is necessary to lower the combustion temperature to reduce particle agglomeration.

Researchers studied the effect of NaCl as a diluent on

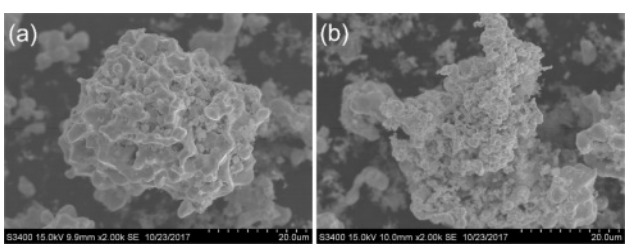

Fig. 17. Morphology of powders composed of (a) (Zr, Ta)B_2 and (b) (Zr, Ta)B_2-TaB_2 phases [99].

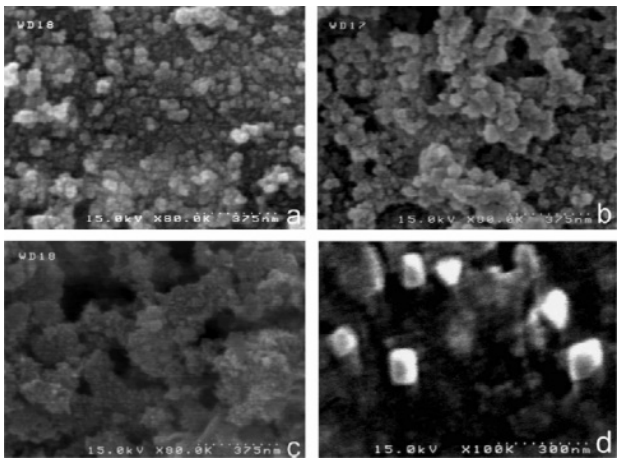

Fig. 18. SEM micrographs of combustion synthesis TiB_2 with various amounts of 0.5KCl-0.25NaCl-0.25$CaCl_2$ mixed salts: (a) 0%, (b) 30%, (c and d) 45% [101].

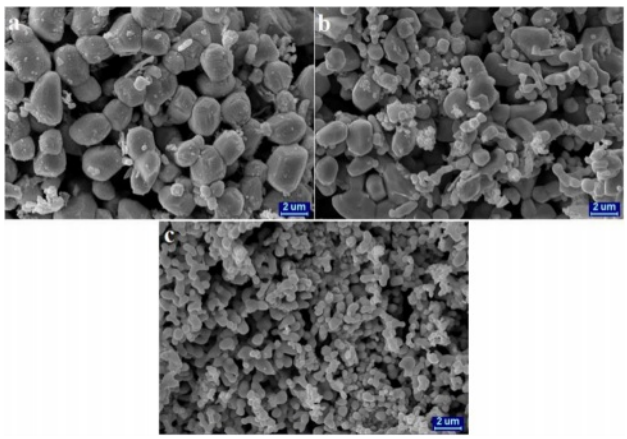

Fig. 19. SEM micrographs of ZrB_2 obtained by adding different additional Mg concentrations: (a) y = 2.5, (b) y = 4.5, (c) y = 9 [102].

powder characteristics. Professor La [100] added the diluent NaCl to the mixed precursor and prepared the submicron TiB_2 powder by the self-propagating high-temperature synthesis method. The results showed that the additional amount of diluent had a significant influence on the sample morphology, particle size, and phase. With the increase of NaCl content, the average particle size of TiB_2 powder decreased from 496 nm to 268 nm. When the amount of NaCl in the raw material was 0.5, 1.0, 1.5, and 2.0 mol, the impurity of $Mg_3B_2O_6$ in the leaching products was very few, and the purity of the product was over 98%. It is worth noting that if an excessive amount of diluent is added, it will directly stop the entire reaction process. Therefore, thermodynamic calculations and kinetic simulations should be done in advance to determine the effective amount of the diluent. Firoozi et al. [101] chose salt mixture of 0.5KCl-0.25NaCl-0.25$CaCl_2$ as a low melting temperature diluent to synthesize the nano-sized TiB_2 powder. The results revealed that 45% salts mixture led to the smallest average particle size of ~90 nm. Thermal analysis of the process indicated that the addition of the low melting temperature salts mixture led to a significant decrease in ignition and combustion temperatures. Meantime, kinetic analysis manifested that formation of a liquid salt phase that improved heat and mass transfer between the reactants.

The researchers studied the effects of Mg and B_2O_3 on ZrB_2 powders in magnesium thermal reduction system. Omran et al. [102] studied the self-propagating high-temperature synthesis characteristics of $2WO_3$-$(1+x)B_2O_3$-$(9+y)$Mg system using H_3BO_3 as boron oxide source. By adding different contents of B_2O_3 and Mg as diluents, the adiabatic temperature and reaction speed can be controlled, as well as inhibiting crystal grain growth and reducing the particle size of the product. A composite powder of tungsten-containing boride was synthesized. It can be seen from Fig. 19 that as the concentration of additional Mg increases, the average particle size of the product decreases slightly. When y increased to 9, the particle size of the powder is significantly reduced from 2 μm to less than 1 μm. However, compared with NaCl diluent, the effect of Mg is much worse. Magnesium directly participates in the reaction as a reducing agent and provides enough heat for the reaction. Excessive magnesium can act as a diluent, but its ability is limited. Therefore, there may be better results when adjusting amounts of NaCl and Mg at the same time in magnesium thermal reduction system.

Ma et al. [103] proposed a simple molten salt process for preparing pure-phase h-ZrB_2 crystallites without using any protective atmosphere at 800 °C. Fig. 20 displays that the products have rose-like particle morphology with nano-scale lamellar structure and the h-ZrB_2 width of a single flake is 200 nm. Research shows that to get good crystallinity of pure-phase h-ZrB_2, the weight ratios of KCl to Zr-B mixture is not less than 4:1, insufficient KCl cannot guarantee to set up an enough and homogeneous liquid environment to isolate air for preventing products from oxidizing. Melting KCl has a great influence on the crystallization process of h-ZrB_2, which is related to the viscosity of the molten medium. Besides, in addition to accelerating the diffusion rate of reactants and promoting chemical

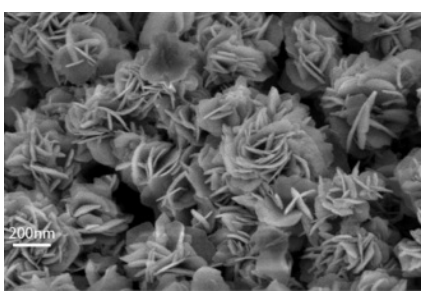

Fig. 20. SEM images of h-ZrB_2 crystallites were prepared by molten salt method at 800 °C [103].

reactions, the KCl melt can also isolate air and prevent the oxidation of h-ZrB_2. The method is simple, environmentally friendly, low-cost, and suitable for large-scale preparation of h-ZrB_2 powder.

Through the above research status, some problems existing in the current researches are found. (i) The powder prepared by most studies has low purity, coarse particle size, and serious agglomeration. (ii) The preheating temperature of the most preparation process is too high. (iii) Adding salt as a diluent based on high-temperature self-propagating combustion synthesis process can effectively reduce the size of powder particles, but there are few kinds of literatures investigated on the mechanism of the diluent and magnesium powder. (iv) Most of the studies were conducted based on small-scale synthesis (under 100 g), lacking data support for large-scale (over 500 g) preparation of high-purity and ultrafine powder. In conclusion, SHS has the advantages of simple process, low cost, and high yield, and is very suitable for large-scale preparation of high-temperature ceramic materials such as carbides and borides. For the shortcomings of the SHS process, there are currently two measures, namely thermodynamics and kinetics. From the perspective of kinetics, reducing the adiabatic temperature of the system is the key to solving problem, which can be usually solved by selecting a suitable reaction system or adding an inert diluent. From the perspective of kinetics, insufficient solid-phase combustion is due to the low particle mobility of the components in the initial mixture and insufficient contact between particles. First, ball milling, microwave, etc. can be used to provide kinetic energy for particle migration or to improve the chemical activities of interfacial particles. In addition, the introduction of the liquid or gas phase during the reaction can reduce the energy barrier that restricts particle migration and increase the contact between particles.

Conclusion

The research of boride and carbide powder has been carried out for a long time, from military to civilian use, from being a raw material to become the main material. With the continuous expansion of its application fields, the requirements for its particle size, purity, microscopic morphology, and functional properties are getting higher and higher. Thereby, the preparation of boride and carbide powders will continue to develop toward more controllable, convenient, and targeted aspects, and their functionality will become more diverse. Especially for the large-scale preparation of nano-powders, it is the most basic requirement to increase the yield while ensuring its high purity and controllable particle size, and it is also a very challenging task. At this stage, most of the preparation methods are difficult to meet these requirements at the same time. There are many problems which are mainly originated from two aspects. On the one hand, the preparation method is not perfect, it is difficult to meet the requirements of particle size and purity at the same time; on the other hand, it is difficult to realize large-scale processes, such as complex equipment, harsh preparation conditions, and high cost. Therefore, the current breakthrough direction is to combine multiple methods based on the advantages of each method to improve the inherent shortcomings of the method itself. For example, combining MA and SHS can improve the problem of uneven mixing of various raw materials in solid-phase reactions. In summary, the future improvement of the powder preparation process should ensure the high purity, controllable particle size (nanoscale), large-scale and low cost.

Acknowledgments

This work was supported by the Science and Technology Fund Plan of Gansu Province (20JR10RA201), the Tamarisk Outstanding Young Talents Program of Lanzhou University of Technology, and the fund of the State Key Laboratory of Advanced Processing and Recycling of Non-Ferrous Metals, Lanzhou University of Technology (SKLAB02019010).

References

1. J.J. Xu, T.T. Yang, Y. Yang, Y.H. Qian, M.S. Li, and X.H. Yin, Corros. Sci. 132 (2018) 161-169.
2. G.S. An, J.S. Han, J.U. Hur, and S.C. Choi, Ceram. Int. 43[8] (2017) 5896-5900.
3. J. Hu, H. Peng, C. Hu, W. Guo, X. Tian, and Y.J. Peng, J. Ceram. Process. Res. 18[1] (2017) 79-85.
4. L.M. Rueschhoff, C.M. Carney, Z.D. Apostolov, and M.K. Cinibulk, Int. J. Ceram. Eng. Sci. 2[1] (2020) 22-37.
5. Y. Cheng, Y. Qi, P. Hu, S. Zhou, G. Chen, J. An, K. Jin, and W. Han, J. Am. Ceram. Soc. 99[6] (2016) 2131-2137.
6. Z. Xie, T. Zhang, R. Liu, Q. Fang, S. Miao, X. Wang, and C. Liu, Int. J. Refract. Met. Hard Mater. 51 (2015) 180-187.
7. J. Xu, Z. Li, S. Xu, P. Munroe, and Z.H. Xie, J. Power Sources 297 (2015) 359-369.
8. Z.I. Zaki, S.H. Alotaibi, M. Alsawat, and B.A. Alhejji, J. Ceram. Process. Res. 22 (2021) 455-460.
9. L. Zoli, A.L. Costa, D. Sciti, Scripta Mater. 109 (2015) 100-103.
10. K.S. Campos, G.F.L. e Silvab, E.H. Nunes, and W.L. Vasconcelos, J. Ceram. Process. Res. 15[6] (2014) 403-407.
11. H.E. Camurlu, Mach. Technol. Mater. 13[9] (2019) 414-416.
12. Y.J. Zhang, J. Wang, Y. Yang, and L. Li, J. Ceram. Process. Res. 20[1] (2019) 90-94.
13. B.R. Golla, A. Mukhopadhyay, B. Basu, and S.K. Thimmappa, Prog. Mater. Sci. 111 (2020) 100651-100723.
14. M.J. Langenderfer, Y. Zhou, J. Watts, W.G. Fahrenholtz, and C.E. Johnson, Ceram. Int. 48[4] (2022) 4456-4463.
15. S.K. Mahmoodi, M. Sharifitabar, and M.S. Afarani, Ceram. Int. 47[3] (2021) 3911-3919.

16. Y.H. Yun, Journal of Ceramic Processing Research 23[3] (2022) 247-251.
17. L. Xu, W.M. Guo, Q.Y. Liu, Y. Zhang, L.X. Wu, Y. You, and H.T. Lin, J. Am. Ceram. Soc. 105[5] (2022) 3133-3140.
18. J.H. Lee and H.K. Park, J. Ceram. Process. Res. 22[5] (2021) 590-596.
19. V.V. Kurbatkina, E.I. Patsera, E.A. Levashov, and A.N. Timofeev, J. Eur. Ceram. Soc. 38[4] (2018) 1118-1127.
20. L. Gao, Y. Zhang, X. Yang, Y.B. He, and L.H. Song, J. Ceram. Process. Res. 21[6] (2020) 615-621.
21. H.M. Kim, S.C. Choi, Y. Kim, H.I. Lee, and K. Choi, J. Ceram. Process. Res. 21[1] (2020) 92-98.
22. J.S. Choi, J.H. Kim, J.U. Hur, S.C. Choi, and G.S. An, J. Ceram. Process. Res. 21[3] (2020) 351-357.
23. F. Li and X. Huang, J. Eur. Ceram. Soc. 38[4] (2018) 1103-1111.
24. H. Zhang, M. Ge, H.F. Zhang, W.J. Kong, S.Q. Yu, and W.G. Zhang, J. Am. Ceram. Soc. 104[4] (2021) 1633-1640.
25. A. Da, F. Long, J. Wang, W. Xing, Y. Wang, F. Zhang, W. Wang, and Z. Fu, J. Wuhan Univ. Technol. 30[4] (2015) 729-734.
26. X. Zou, K. Zheng, X. Lu, Q. Xu, Z. Zhou, Faraday Discuss. 190 (2016) 53-69.
27. P. La, S. Han, X. Lu, Y. Wei, J. Inorg. Mater. 29[2] (2014) 191-196.
28. A.S. Mukasyan, Y.C. Lin, A.S. Rogachev, D.O. Moskovskikh, J. Am. Ceram. Soc. 96[1] (2013) 111-117.
29. T. Tsuchida, S. Yamamoto, J. Mater. Sci. 42[3] (2007) 772-778.
30. S. Ruiying, L. Ning, Z. Hongqin, L. Zhongwei, C. Wei, Cemented Carbide, 26[2] (2009) 74-80.
31. Y. Zhou, T.W. Heitmann, W.G. Fahrenholtz, G.E. Hilmas, J. Eur. Ceram. Soc. 39[8] (2019) 2594-2600.
32. H.-Y. Qiu, W.-M. Guo, J. Zou, G.-J. Zhang, Powder Technol. 217 (2012) 462-466.
33. B.N. Chandran, D. Devapal, P. Prabhakaran, Ceram. Int. 45[18] (2019) 25092-25096.
34. L. Feng, S. Lee, H. Lee, Int. J. Refract. Met. Hard Mater. 64 (2017) 98-105.
35. J. Li, Z. Fu, W. Wang, H. Wang, S. Lee, K. Niihara, Ceram. Int. 36[5] (2010) 1681-1686.
36. L. Peiqing, H. Shaobo, L. Xuefeng, J. Qian, W. Yupeng, Powder Metall. Technol. 31[1] (2013) 3-8.
37. X. Ke, Z. Faqi, Z. Hua, A. Ning, W. Haokai, Z. Min, Z. Yuehong, L. Peinqing, J. Funct. Mater. 52[11] (2021) 10177-10186.
38. F. Li, C. Tan, J. Liu, J. Wang, Q. Jia, H. Zhang, and S. Zhang, Ceram. Int. 45[7] (2019) 9611-9617.
39. M. Emamalizadeh, M. Mahdavi, and A. Shokrolahi, J. Mater. Res. Technol. 9[4] (2020) 7686-7700.
40. F. Arianpour, F. Kazemi, and H.R. Rezaie, J. Australian Ceram. Soc. 56[3] (2020) 969-977.
41. Y. Zhang and H. Sun, J. Ceram. Process. Res. 19[4] (2018) 355-359.
42. Y. Miao, X. Wang, P. Firbas, K. Wang, Z. Yang, B. Liang, Y.-B. Cheng, and D. Jia, J. Sol-Gel Sci. Technol. 77[3] (2016) 636-641.
43. L. Telmenbayar and J. Temuujin, J. Ceram. Process. Res. 17[5] (2016) 489-493.
44. D. Davoodi, S. Hassanzadeh-Tabrizi, A.H. Emami, and S. Salahshour, Ceram. Int. 41[7] (2015) 8397-8401.
45. S. Hassanzadeh-Tabrizi, D. Davoodi, A.A. Beykzadeh, and S. Salahshour, Ceram. Int. 42[1] (2016) 1812-1816.
46. T. Tsuchida and S. Yamamoto, J. Eur. Ceram. Soc. 24[1] (2004) 45-51.
47. J.-X. Wang, D.-W. Ni, S.-M. Dong, G. Yang, Y.-F. Gao, Y.-M. Kan, X.-W. Chen, Y.-P. Cao, and X.-Y. Zhang, RSC Adv. 7[37] (2017) 22722-22727.
48. Y. Li, W. Han, H. Li, J. Zhao, and T. Zhao, Mater. Lett. 68 (2012) 101-103.
49. X.Y. Tao, W.F. Qiu, H. Li, and T. Zhao, Chinese Chem. Lett. 21[5] (2010) 620-623.
50. C. Xie, M. Chen, X. Wei, M. Ge, and W. Zhang, J. Am. Ceram. Soc. 95[3] (2012) 866-869.
51. I. Borovinskaya, A. Gromov, E.A. Levachov, Y. Maksimov, A. Mukasyan, and A.S. Rogachev, "Concise Encyclopedia of Self-propagating High-temperature Synthesis: History, Theory, Technology, and Products", Elsevier, 2017:
52. Z.A. Munir and U. Anselmi-Tamburini, Mater. Sci. Rep. 3[7-8] (1989) 277-365.
53. C. Liu, X. Chang, Y. Wu, X. Li, Y. Xue, X. Wang, and X. Hou, Ceram. Int. 46[6] (2020) 7099-7108.
54. C. Zeng, K. Tong, M. Zhang, Q. Huang, Z. Su, C. Yang, X. Wang, Y. Wang, and W. Song, Ceram. Int. 46[4] (2020) 5244-5251.
55. S.N. Katea, L. Riekehr, and G. Westin, J. Eur. Ceram. Soc. 41[1] (2021) 62-72.
56. X. Sun, C. Deng, J. Ma, X. Zhao, S. Hao, Z. Li, and B. Liu, J. Mater. Sci. 53[20] (2018) 14149-14159.
57. M. Liang, F. Li, X. Ma, Z. Kang, X. Huang, X.-G. Wang, and G.-J. Zhang, Ceram. Int. 42[1] (2016) 1345-1351.
58. N. Patra, D.D. Jayaseelan, and W.E. Lee, J. Am. Ceram. Soc. 98[1] (2015) 71-77.
59. M. Umalas, I. Hussainova, V. Reedo, D.-L. Young, E. Cura, S.-P. Hannula, R. Lõhmus, and A. Lohmus, Mater. Chem. Phys. 153 (2015) 301-306.
60. F. Li, X. Huang, and G.-J. Zhang, Ceram. Int. 41[2] (2015) 3335-3338.
61. Y. Miao, F. Zhang, M. Huang, G. Shi, and H. Huang, "Synthesis of Ultra-High Temperature ZrC Ceramic Powder by Sol-Gel and Spark Plasma Sintering Method Conference Paper", IOP Conference Series: Materials Science and Engineering: IOP Publishing, 2019, p. 012003.
62. Y. Zhou, T.W. Heitmann, E. Bohannan, J.C. Schaeperkoetter, W.G. Fahrenholtz, and G.E. Hilmas, J. Am. Ceram. Soc. 103[4] (2020) 2891-2898.
63. C. Musa, R. Licheri, R. Orrù, G. Cao, D. Sciti, L. Silvestroni, L. Zoli, A. Balbo, L. Mercatelli, M. Meucci, and E. Sani, Materials 9[6] (2016) 489-504.
64. L. Yu, L. Feng, H.I. Lee, L. Silvestroni, D. Sciti, Y.J. Woo, and S.-H. Lee, Int. J. Refract. Met. Hard Mater. 81 (2019) 149-154.
65. A. Moon, C.Y. Suh, J. Kim, and H. Kwon, J. Alloys Compd. 740 (2018) 82-87.
66. D. Davoodi, M. Tayebi, A.H. Emami, R. Miri, and S. Salahshour, Mater. Chem. Phys. 222 (2019) 351-360.
67. X.F. Wang, J.C. Liu, F. Hou, J.D. Hu, X. Sun, and Y.C. Zhou, J. Am. Ceram. Soc. 98[1] (2015) 197-204.
68. S. Cetinkaya, J. Am. Ceram. Soc. 100[12] (2017) 5444-5449.
69. H. Liu, Y. Cai, Q. Xu, H. Liu, Q. Song, and Y. Qi, RSC Adv. 7[4] (2017) 2301-2307.
70. J.P. Yasnó, R.F. Gunnewiek, and R.H. Kiminami, Adv. Powder Technol. 30[7] (2019) 1348-1355.
71. S. Murthy, M. Patel, J. Reddy, and V. Bhanu Prasad, Trans. Indian Inst. Met. 71[1] (2018) 57-65.

72. Z. Chen, X. Zhao, M. Li, H. Wang, Q. Li, G. Shao, W. Liu, H. Xu, H. Lu, and R. Zhang, Ceram. Int. 45[11] (2019) 13726-13731.
73. L. Ma, J. Yu, X. Guo, Y. Zhang, Y. Feng, H. Zong, Y. Zhang, and H. Gong, Ceram. Int. 43[15] (2017) 12975-12978.
74. X. Lian, X. Hua, X. Wang, L. Deng, and L. Zhang, "Effect of Carbon Source on the Synthesis of ZrB_2-SiC Composite Powders Conference Proceedings", IOP Conference Series: Materials Science and Engineering: IOP Publishing, 2020, p. 012095.
75. L. Bai, S. Ni, H. Jin, J. He, Y. Ouyang, and F. Yuan, Int. J. Appl. Ceram. Technol. 15[2] (2018) 508-513.
76. Y.L. Krutskii, T. Krutskaya, and E. Kisorets, Mater. Today: Proc. 31 (2020) 486-488.
77. M. Li, C. Ke, and J. Zhang, J. Alloys Compd. 834 (2020) 155062-155084.
78. Y. Wang, Y.-D. Wu, K.-H. Wu, S.-Q. Jiao, K.-C. Chou, and G.-H. Zhang, Int. J. Min. Met. Mater. 26[7] (2019) 831-838.
79. S. Song, R. Li, L. Gao, C. Sun, P. Hu, and Q. Zhen, Ceram. Int. 44[5] (2018) 4640-4645.
80. W. Guo, D. Tan, L. Zeng, H. Lin, and C. Wang, Ceram. Int. 44[4] (2018) 4473-4477.
81. W. Guo, L. Wu, S. Sun, and H. Lin, J. Am. Ceram. Soc. 100[2] (2017) 524-528.
82. H. Moayyeri, R. Mehdinavaz Aghdam, R. Ghelich, and F. Golestani-fard, Adv. Appl. Ceram. 117[3] (2018) 189-195.
83. J. He, Y. Gao, Y. Wang, J. Fang, and L. An, Ceram. Int. 43[1] (2017) 1602-1607.
84. F. Li, Y. Cao, J. Liu, H. Zhang, and S. Zhang, Ceram. Int. 43[10] (2017) 7743-7750.
85. B. Xie, L. Ma, D. Gao, X. Lin, Y. Liu, Y. Zhang, and H. Gong, Ceram. Int. 44[8] (2018) 8795-8799.
86. A.M. Stolin, P.M. Bazhin, A.S. Konstantinov, A.P. Chizhikov, E.V. Kostitsyna, and M.Y. Bychkova, Ceram. Int. 44[12] (2018) 13815-13819.
87. R. Licheri, C. Musa, R. Orrù, G. Cao, D. Sciti, and L. Silvestroni, J. Alloys Compd. 663 (2016) 351-359.
88. M. Baris, T. Simsek, T. Simsek, S. Ozcan, and B. Kalkan, Adv. Powder Technol. 29[10] (2018) 2440-2446.
89. J. Ban, C. Zhou, L. Feng, Q. Jia, X. Liu, and J. Hu, Ceram. Int. 46[7] (2020) 9817-9825.
90. H. Morito, K. Koshiji, and H. Yamane, J. Asian Ceram. Soc. 5[4] (2017) 479-481.
91. Y. Lin, J. Liu, S. Song, J. Liu, S. Bashir, Y. Guo, and Q. Zhen, Ceram. Int. 45[3] (2019) 4016-4021.
92. A. Merzhanov and I. Borovinskaya, Combust. Sci. Technol. 10[5-6] (1975) 195-201.
93. P. Ronsheim, L. Toth, A. Mazza, E. Pfender, and B. Mitrofanov, J. Mater. Sci. 16[10] (1981) 2665-2674.
94. V. Balouchi, F.S. Jazi, and A. Saidi, J. Ceram. Process. Res. 16[5] (2015) 605-608.
95. E. Levashov, A. Mukasyan, A. Rogachev, and D. Shtansky, Int. Mater. Rev. 62[4] (2017) 203-239.
96. Y. Bao, L. Huang, Q. An, S. Jiang, R. Zhang, L. Geng, and X. Ma, J. Eur. Ceram. Soc. 40[13] (2020) 4381-4395.
97. J. Li, Z.Y. Fu, W.M. Wang, H. Wang, S. Lee and, K. Niihara, J. Chinese Ceram. Soc. 38[5] (2009) 979-985.
98. M. Zhang, B. Huang, Q. Hu, and J. Li, Int. J. Refract. Met. Hard Mater. 31 (2012) 230-235.
99. V. Kurbatkina, E. Patsera, E. Levashov, and A. Timofeev, J. Eur. Ceram. Soc. 38[4] (2018) 1118-1127.
100. L. Peiqing, O. Yujing, H. Shaobo, L. Xuefeng, and W. Yupeng, J. Mater. Eng. 43[7] (2015) 14-20.
101. A. Nekahi and S. Firoozi, Mater. Res. Bull. 46[9] (2011) 1377-1383.
102. J.G. Omran, M. Sharifitabar, and M.S. Afarani, Ceram. Int. 44[12] (2018) 14355-14362.
103. J. Ma, S. Cao, T. Li, Q. Chen, and D. Zhang, Mater. Sci. Eng.: B 261 (2020) 114698-114701.